Available online at https://link.springer.com/journal/42241
http://www.jhydrodynamics.com
Journal of Hydrodynamics, 2021, 33(1): 74-85
https://doi.org/10.1007/s42241-021-0013-0

Liutex-based vortex control with implications for cavitation suppression *

Yi-qian Wang[1], Hai-dong Yu[2], Wei-wen Zhao[3], De-cheng Wan[3]
1. *School of Mathematical Science, Soochow University, Suzhou 215006, China*
2. *School of Aerospace Engineering, Tsinghua University, Beijing 100084, China*
3. *Computational Marine Hydrodynamics Lab (CMHL), State Key Laboratory of Ocean Engineering, School of Naval Architecture, Ocean and Civil Engineering, Shanghai Jiao Tong University, Shanghai 200240, China*

(Received December 25, 2020, Revised February 26, 2021, Accepted February 27, 2021, Published online March 5, 2021)

Abstract: Viewed as sinews and muscles of fluid motion, coherent vortical structures with their interactions are key to understanding the flow dynamics. Based upon this observation, we explore the possibility of efficient flow control by directly manipulating vortices numerically inside the flow field based on the vortex definition and identification system of Liutex. The objective is twofold: (1) to study the vortex dynamics, for example, by observing the response of the flow to strengthening or weakening of certain vortices, and (2) to obtain efficient vortex-based control strategies which might lead us to practical applications. In the present numerical study, the manipulating of vortices is achieved by introducing additional source (force) terms to the Navier-Stokes equations, which hereafter will be collectively called Liutex force field model. Methodologies including controlling the rotation strength and centripetal force of particular vortices are detailed in a flow past a cylinder with different control purposes at Reynolds number of 200. Further examples are provided with a cavitating flow around two-dimensional Clark-Y hydrofoil, with particular interests on cavitation suppression. It is illustrated particular vortex with cavitation encircled could be effectively suppressed.

Key words: Vortex dynamics, Liutex vector, flow control, cavitation

Introduction

Cavitation, a common phenomenon in hydraulic machinery such as turbines and pumps, generally results from the reduction of pressure to or below the saturated vapor pressure with small vaporized cavities formed in the liquids, and is often accompanied by detrimental effects including vibrations, noise, damage to components and a loss of efficiency[1-2]. Due to the engineering importance, experimental and numerical investigations on cavitation have been constantly carried out to reveal the mechanisms of the inception, development and collapse of cavitation, the last of which, if happed near to a metal surface, could result in surface fatigue of metal called "cavitation erosion". With intricate problems involved, like unsteadiness, multiphase, turbulence and compressibility, however, cavitation remains a challenging issue, especially in terms of control. The influence of geometry, blade number for propellers and other parameters on cavitation had been widely studied with optimization for better hydraulic efficiency and pressure fluctuation alleviation[3-4]. Devices like micro vortex generator have also been installed at appropriate places to suppress cavitation[5-6]. However, further investigations in cavitation mechanisms and more efficient control strategies are still necessary especially with the engineering importance of cavitation. In this study, we focus on the kind of cavitation, or the part of the cavitating flow that is directly associated with vortices, and explore that the possibility of using vortex-based force field models to achieve cavitation suppression.

Ubiquitously seen in both nature and engineering, vortex serves as building blocks of fluid flows and turbulence[7-8]. Therefore, the definition and visualization of vortices are of great importance. According to Liu et al.[9], vortex identification methods can be classified into three generations. The first-generation methods are based on vorticity, which generally relates vorticity filaments/tubes or vorticity concentrations to vortices. However, these efforts had been

* Project supported by the National Nature Science Foundation of China (Grant Nos. 11702159, 51879159 and 51909160).
Biography: Yi-qian Wang (1987-), Male, Ph. D., Associate Professor, E-mail: yiqianw@sina.com
Corresponding author: De-cheng Wan, E-mail: dcwan@sjtu.edu.cn

challenged by many researchers that the correlation between vortex and vorticity can be very weak, especially in the near wall region of turbulence[10-11]. To overcome the issue, multiple scalar-valued vortex visualization methods have been introduced, including Q, λ_2, Δ, λ_{ci} and other methods[12-15]. The scalar parameters of these methods all somewhat represent the swirling strength of vortices, but are different from each other. Moreover, the physical meanings of these parameters are unclear with different dimensions. With these methods, vortices are generally visualized as iso-surfaces which requires an arbitrarily selected threshold. More importantly, these methods have the shear contamination problem, i.e., identifies vortex from pure shear flows. Classified as the second generation, these scalar methods have not provided a unique and unambiguous definition of vortices. These difficulties prompted the development of the third-generation vortex identification method: Liutex. The Liutex vector was introduced by Liu et al.[16] to represent the rigid rotation part of fluid motion, with its direction as the rotational axis and magnitude as twice the angular velocity of rigid rotation. Based on the Liutex vector, multiple methods have been proposed to illustrating vortices from different perspectives, including Liutex magnitude iso-surface, object Liutex[17], Liutex-Ω methods[18-19], and Liutex core line method[20-21], etc. which collectively have been proven efficient in capturing vortices in various flows. Substantial progresses have been made both in theoretical and application aspects ever since[22-24].

One important feature of the Liutex system is its capability of providing the six core elements of vortex, namely, absolute strength, relative strength, local rotation axis, vortex rotation axis, vortex core size and vortex boundary, which are introduced to be touchstones to test vortex definition and visualization methods. (1) the absolute strength is actually the Liutex magnitude, which represents twice the angular speed of the rigid rotation part of the fluid motion. (2) the relative strength is given by the parameter of the Liutex-Ω method, which could be understood as the density of Liutex over vorticity or the rigidity of fluid motion. Using relative strength could capture both strong and weak vortices at the same time. (3) The local rotational axis is the direction of the Liutex vector, about which the local fluids rotate. It is this distinctive feature that separate Liutex from other second-generation methods as they are all scalar valued without a direction. (4) The vortex rotation axis or the global axis is defined as the connected points that satisfies $\nabla R \times \boldsymbol{r} = 0$ and $R > 0$, which has been introduced as Liutex core line method to extract vortex cores. (5) The vortex core size can be defined as a place where the relative rotational strength declined with 95% of the corresponding vortex core center point. (6) The boundary of a vortex is proposed to be $\Omega_R = 0.52$, which can be applied to various flows without adjustment of thresholds. The six core elements provided by Liutex system thoroughly describe the vortices from multiple perspectives, which has not been possible with previous vortex identification methods.

The idea that vortices are the "sinews and muscles of fluid motion"[6] prompts researchers to couple certain reduced-order representations of vortices, the so called point vortices and vortex blobs for example, and methods of control and optimization theory[25-26]. However, the reduced-order models are generally based on vorticity or flow patterned deduced directly from velocity field, and thus hardly represent the actual vortices exactly. In addition, investigations in this regard are generally related to dynamical systems and limited to simple flow configurations and difficult to generalize. On the other hand, almost no vortex-based control strategies based on the second generation of vortex identification methods have been developed, due to the inability of scalar-valued criteria to thoroughly describe the actual vortices, such as providing the six core elements. Based on the Liutex system, Yu and Wang[27] explored the possibility of directly numerically manipulating vortices and thus obtain vortex dynamics and deduct control strategies. Two methodologies, centripetal force field model and counter-rotation force field model, were proposed to be added in the control equations, which directly exerted in the vortex regions to modify the vortices. A specifically explored issue in that research is the relationship between vortices and low-pressure minimums, which relates to the issue of cavitation in hydrodynamics. It is well known that cavitation generally occurs given the local fluid pressure is under the saturated vapor pressure, and then phase transformation from water to vapor happens and bubbles appear. Cavitation is always accompanied by vibration and noise, efficiency loss and erosion, which poses great changes to hydraulic machinery[1-2]. Despite the engineering importance of cavitation, few researches touched upon the issue of cavitation control or suppression. Based on the fact that use of Liutex-based vortex force field to control the flow field can alter the pressure and the vortices, it is attempting to investigate whether those models can be used to suppress cavitation.

In this paper, we first review the definition of Liutex and Liutex-based force field models, which are then applied to a flow past a circular cylinder with Reynolds number 200. Finally, the models are applied to a cavitating vortex in a flow past Clark-Y hydrofoil with cavitation number of 0.8. The possibility of cavitation suppression by Liutex-based vortex control is then discussed with conclusions.

1. The definition of Liutex vector

The local structure of flow topology is determined by velocity gradient tensor, which is the reason why most vortex identification methods are based on the velocity gradient tensor, and so is the Liutex vector. A distinctive feature of Liutex is that it includes the directional information, i.e., the local rotational axis. It is pointed out that the local axis is the real eigenvector of the velocity gradient tensor given that the other two corresponding eigenvalues are complex conjugate[28]. An explicit expression for the Liutex vector is then derived[29]

$$\boldsymbol{R} = R\boldsymbol{r} = \left[\boldsymbol{\omega}\cdot\boldsymbol{r} - \sqrt{(\boldsymbol{\omega}\cdot\boldsymbol{r})^2 - 4\lambda_{ci}^2}\right]\boldsymbol{r} \tag{1}$$

where $\boldsymbol{\omega}$ is the vorticity vector, λ_{ci} is the imaginary part of the complex eigenvalue and $\boldsymbol{r}$ is the real eigenvector of the velocity gradient tensor.

Initially, the Liutex vector was introduced by rotation to a special coordinate we denote as principal coordinate. This coordinate rotation approach is more intuitive in prompting the systematic decomposition of fluid motion, while the explicit formula of Liutex is also physical revealing and brings computational efficiency improvement. Therefore, both approaches are indispensable and could be found in Liu et al.[9], Wang et al.[22]

2. The Liutex force field model

A local pressure minimum can be often found inside a vortex, which can be understood as the pressure gradient towards the rotation center provides the centripetal force for the fluids to rotate. The centripetal force model is thus proposed to control the pressure minimum inside vortices[27]. First, we identify the vortex center P_0. Then consider another point P inside the vortex region, we thus can obtain the vector pointing from P_0 to P and name it as $\boldsymbol{l}$ which serves as the global rotation radius. The angular velocity of the rigid rotation part of point P is taken as half the Liutex, i.e., $\boldsymbol{R}/2$. With radius and angular velocity defined, centripetal force (actually centripetal acceleration) can be calculated by

$$\boldsymbol{a} = \frac{\boldsymbol{R}}{2}\times\left(\frac{\boldsymbol{R}}{2}\times\boldsymbol{l}\right) = \frac{1}{4}\boldsymbol{R}\times(\boldsymbol{R}\times\boldsymbol{l}) \tag{2}$$

Thus, we can add the centripetal force as a source term in the incompressible Navier-Stokes equation

$$\frac{\partial\boldsymbol{u}}{\partial t} + (\boldsymbol{u}\cdot\nabla)\boldsymbol{u} = -\nabla\frac{p}{\rho} + \nabla\cdot(\nu\nabla\boldsymbol{u}) \pm \boldsymbol{a} \tag{3}$$

where $\boldsymbol{u}$ is the velocity vector while p, ρ and ν represent pressure, density and kinematic viscosity respectively. For compressible flow or multiphase flow with different density, the centripetal forces added to corresponding equation would be $\boldsymbol{a}$ multiplied by ρ.

A second and more intuitive approach would be adding source terms in the Navier-Stokes equation to drive the fluids rotating in the counter direction to the rotational direction of vortices identified by Liutex system. The first step would be again to recognize the vortex cores. Then form a vector $\boldsymbol{l}$ from corresponding center P_0 to the considered point P in the vortex region. With Liutex as twice the angular velocity of rigid rotation part of the flow, the rigid rotation velocity part can be obtained as

$$\boldsymbol{U} = \frac{\boldsymbol{R}}{2}\times\boldsymbol{l} \tag{4}$$

With an addition time scale τ, we can define a new force (acceleration) model

$$\boldsymbol{a} = -\frac{\boldsymbol{U}}{\tau} = -\frac{1}{2\tau}\boldsymbol{R}\times\boldsymbol{l} \tag{5}$$

Thus, τ acts like a relaxation time during which the rigid rotation part velocity could be decreased to zero, and the minus sign in Eq. (5) means that the force will always be the opposite of rigid velocity and thus holds back the rotational motion. The main principle to select τ is that it should not be too small to cause numerical instability while should not be too large to be trivial.

3. Flow past a cylinder at Reynolds number of 200

In this part, we are going to detail the application of Liutex force field model to a flow past a cylinder at Reynolds number of 200, which is characterized by the laminar oscillating vortex street. The diameters of the cylinder d is set as 2 m, with the kinematic viscosity $\nu = 0.01\,\mathrm{m}^2/\mathrm{s}$ and inflow velocity $U_\infty = 1\,\mathrm{m/s}$, the Reynolds number is obtained by $Re = U_\infty d/\nu = 200$. The open source platform-OpenFOAM is adopted for numerical simulations, and the uncontrolled case has been validated against the numerical results of Braza et al.[30] on the lift and drag coefficients. Flows around circular cylinder of various Reynolds numbers have been widely studied in that boundary layer, separation, turbulence, vortex street and other important flow phenomena are all presented in this rather simple geometry with practical significance. We select flow of $Re = 200$ to focus

our attention on the wake vortices control and vortex/solid boundary interaction.

3.1 *Centripetal force model*

It has been demonstrated by Yu and Wang[27] for a particular wake vortex that adding and subtracting centripetal forces according to Eq. (2) could attenuate or strengthen the pressure minimum of vortex centers while the vortical structure, represented by Liutex, is basically unchanged, which indicates certain decoupling between the velocity field and pressure inside the considered vortex. However, the control was applied to the particular isolated vortex of interest which had been actually far away from the wall. In addition, since our strategy in identifying vortices is to use local information, like defining the Liutex vector based on velocity gradient, to approximate the global rotation, the mismatch requires us to do a parameter study, i.e., variating the strength of forcing. We introduce an additional parameter α, and thus the new centripetal force is now obtained by

$$\boldsymbol{a}=\frac{\boldsymbol{R}}{2}\times\left(\frac{\boldsymbol{R}}{2}\times\boldsymbol{l}\right)=\frac{1}{4}\alpha\boldsymbol{R}\times(\boldsymbol{R}\times\boldsymbol{l}) \tag{6}$$

The first strategy would be to use Eq. (6) across the whole computational domain. We denote t_0 as the time when the centripetal forces begin to take effect. To detect vortex centers for the current two dimensional case, we use the condition that $\nabla R_z=0$ given that R_z is not trivial. Here, R_z is the Liutex component in the third z direction which is perpendicular to the two axis in the cylinder plane. Of course, we can treat the Liutex vector as a scalar in two dimensional problems. We will, however, insist on using the nomenclatures above to be consistent with both two- and three-dimensional cases. A further requirement on the vortex centers is that the distance between centers rotating clockwise (anti-clockwise) larger than the cylinder diameter, which results from the general distribution of vortices in the considered flow.

Results of the uncontrolled case and the centripetal force model controlled case with $\alpha=1$ and $\alpha=-1$ are shown in Fig. 1 at $t=t_0+0.096T$, where T is the shedding period of the uncontrolled case. As expected, with $\alpha=1$, the additional term $\boldsymbol{a}$ provides part of the centripetal force, thus alleviating the pressure minimum inside vortices. As shown in Fig. 1, the pressure extreme of the red squared vortex increases from $p=-0.730$ in Fig. 1(d) to $p=-0.660$ in Fig. 1(e). Note that here we are using relative pressure as the incompressible Navier-Stokes equation is invoked in simulating. By tracking the

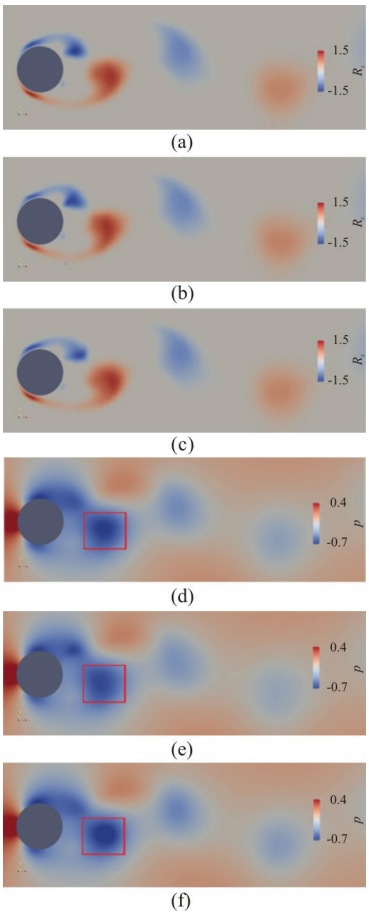

Fig. 1 (Color online) Centripetal force model with $\alpha=\pm1$. The distribution of Liutex component R_z and pressure for the uncontrolled case are shown in (a) and (b), and for the controlled case with $\alpha=1$ are shown in (c) and (d), and for the controlled case with $\alpha=-1$ are shown in (e) and (f)

pressure of one point inside the vortex core, it is found that the amplitude of pressure oscillation range is about 0.35. Thus, the attenuation of the pressure minum is relatively significant to this range as the increasement 0.07 takes up 20% of the oscillation range. Similarly, with $\alpha=-1$, the pressure gradient inside vortices has to provided the centripetal force as well as to overcome the additional term $\boldsymbol{a}$. Thus the pressure minimum of the red quared vortex drops to $p=-0.785$ as shown in Fig. 1(f). Similar conclusions can be drawn for the other wake vortices in the downstream of the red square vortex, which, however, is not obvious from Fig. 1 because of the lengend is mainly selected based on the strong red-squared vortex. On the other hand, it can be seen from Figs. 1(a), 1(b) and 1(c) that the vortical structures represented by Liutex is basically unchanged with α selected as 1 or −1. The above discussions are consistent with the results of Yu and Wang[27].

However, to provide the centripetal force for vortices to rotate is not the only one reason for low pressure regions. For example, despite that we applied the centripetal force model across the whole flow field, including the Liutex concentrations close to the front wall of cylinder, no noticable change of the corresponding pressure distributions can be observed in Figs. 1(d), 1(e) and 1(f).

Although relatively, the flow field, especially the Liutex distribution, is kind of decoupled from the pressure field in the sense that while the centripetal force model significantly alters the pressure field, the vortical structures, on the other hand, basically remains the same, certainly the flow filed must be influenced due to the pressure-velocity coupling according to the incompressible Navier-Stokes equations. It is shown in Fig. 2 the Liutex distribution at $t = t_0 + 47.8T$, at which time obviously the three cases are out of phase. The shedding periods obtained based on the lift coefficient are 10.45 s, 10.55 s and 10.30 s respectively for the uncontrolled case, $\alpha = 1$ case and $\alpha = -1$ case. That is to say in addition to attenuate the pressure drop inside the vortices by adding centripetal force, it also decreases the shedding frequency of the vortex street. On the other hand, subtracting centripetal force deteriorate the situation both by strengthening the pressure drop in the vortex cores and increasing the shedding frequency.

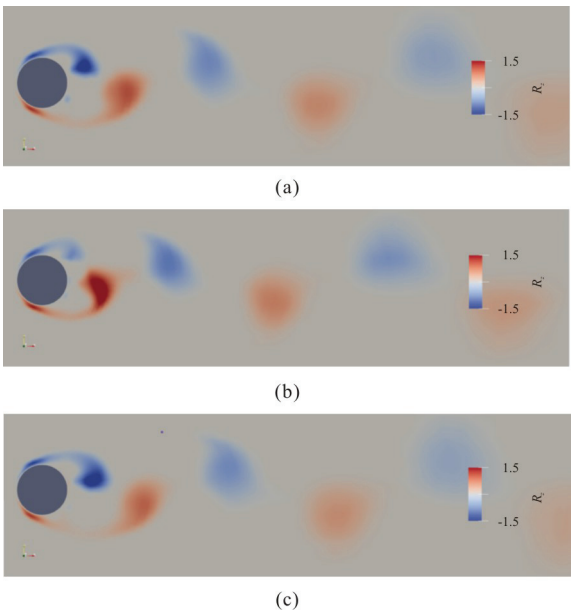

Fig. 2 (Color online) The distribution of Liutex component R_z at $t = t_0 + 47.8T$ for the uncontrolled case (a) and the controlled case with $\alpha = 1$ (b) and $\alpha = -1$ (c)

Because the derived centripetal force is based on the local information, it could not exactly equal to the actual centripetal forced needed. However, from the results above, it seems that the exerted forces have not surpass the actual centripetal forces. Next, we increase the control intensity by adjusting α. The pressure distribution at $t = t_0 + 0.096T$ for multiple values of α is shown in Fig. 3. Obviously, the pressure of the vortex center of the red squared vortex increases as α increases from 2 to 6, despite that pressure minimum has been pushed aside for $\alpha = 4$ and $\alpha = 6$, which indicate that the supplied forces have exceeded the centripetal force needed. A futher evidence is that the vortex adjacent to the red squared vortex downstream now clearly has an positive pressure center with $\alpha = 4$ and $\alpha = 6$ as shown in Figs. 3(b) and 3(c). The trends that the shedding frequany decreases as the centripetal control intensifies has again been confirmed as the shedding period increases from 10.75 s at $\alpha = 2$ to 11.90 s at $\alpha = 4$ to 12.90 s at $\alpha = 6$. The average pressure distribution of the uncontroled case and centripetal force controlled case with $\alpha = 6$ are shown in Fig. 4. It can be seen that not only the instataneous pressure minimums have been alleviated, but also the overall pressure has been increased accordingly. A noticable thing is that as for the case with $\alpha = 6$, the presure minimum inside the vortices near the cylinder wall encircles by the green ellipses in Figs. 3(c) and 4(b) has also been alleviated. Similarly, with magnitude of negative α increases, for example, from $\alpha = -2$ to $\alpha = -4$ and to $\alpha = -6$, the pressure minimum of vortex cores would be continuously strengthened, and accordingly the shedding frequency increases.

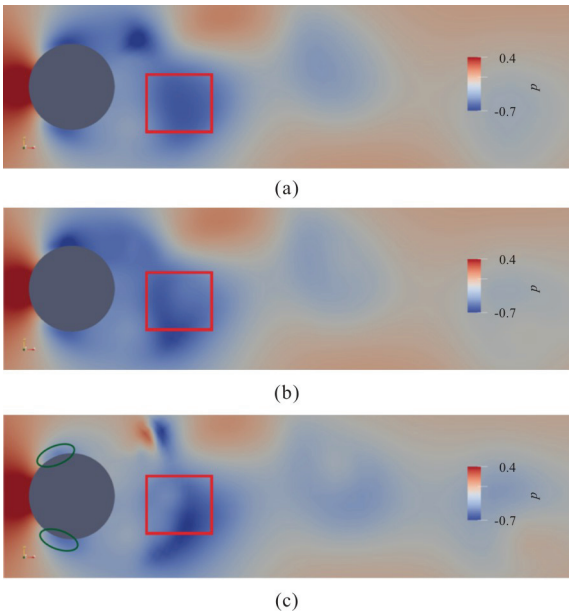

Fig. 3 (Color online) The pressure distribution at $t = t_0 + 0.096T$ with (a) $\alpha = 2$, (b) $\alpha = 4$ and (c) $\alpha = 6$

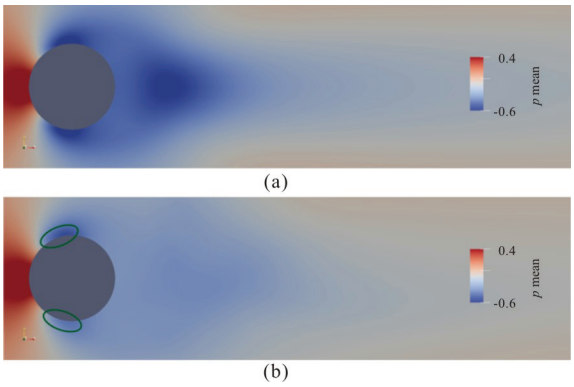

Fig. 4 (Color online) The mean pressure distribution of (a) the uncontrolled case, (b) $\alpha = 6$

As we have noted, with centripetal force model, the vortical structures are only mildly modified with slight change of vortex shedding period. However, as the magnitude of α continues to increase, the force exerted must become dominant over the actual centripetal force, and thus the flow would be significantly altered. As shown in Fig. 5(a) with $\alpha = 10$, the vortex is squeezed which lead the vortex to break into smaller vortices, while for $\alpha = -10$ in Fig. 5(b), however, the vortex is stretched and also breaks. In engineering, effective destruction of wake vortices is of great importance, and possibly intense centripetal force model could be used to construct new methodologies.

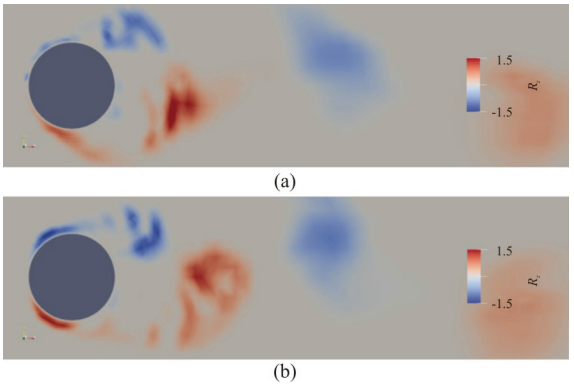

Fig. 5 (Color online) The vortex distribution at $t = t_0 + 0.096T$ with (a) $\alpha = 10$, (b) $\alpha = -10$

3.2 *Counter-rotation force model*

The second Liutex force field model contrived is the counter-rotation force model. We can use the time scale τ in Eq. (5) to adjust the intensity of the control, and by introducing another parameter $\beta = 1/\tau$, thus

$$\boldsymbol{a} = -\frac{\boldsymbol{U}}{\tau} = -\frac{1}{2\tau}\boldsymbol{R}\times\boldsymbol{l} = -\frac{1}{2}\beta\boldsymbol{R}\times\boldsymbol{l} \tag{7}$$

As the shedding period of the uncontrolled case is 10.45 s, we select $\tau = 1\,\mathrm{s}$ to be about 1/10 of the shedding period, and thus $\beta = 1$. And setting $\beta = -1$ means the force will in fact strengthen the detected rotation, which of course is not counter rotation. However, generally it would be preferable if we can weaken the vortices in the flow field, and we persist to use the name counter-rotation model even with β negative. As shown in Figs. 6(c) and 6(e), the vortices immediately weakened with $\beta = 1$ while the vortices immediately strengthened with $\beta = -1$ at $t = t_0 + 0.096T$ compared to the uncontrolled case in Fig. 6(a). In addition, the counter-rotation force ($\beta = 1$) disperses the vortices as the area covered by Liutex get larger. On the other hand, the strengthening process makes the vortices more focused. This phenomenon become more obvious in a later time (about two shedding period later) as shown in Figs. 6(b), 6(d) and 6(f). Especially as shown in Fig. 6(d), the vortices become very weak and dispersed. While for $\beta = -1$, the Liutex distribution is more concentrated than the uncontrolled case because as the rotation gets faster, the centripetal force needed increases which lead to strong pressure gradient that concentrates the vortices.

The pressure and mean pressure distributions for the three cases are shown in Fig. 7, which confirms the discussions above. The dispersion of vortices leads to a more uniform pressure distribution in Fig. 7(b) while the concentration of vortices deteriorates the pressure minimums in Fig. 7(c). Similarly, as shown in Figs. 7(d), 7(e) and 7(f), the low mean pressure has been very much smoothed for the case with $\beta = 1$ while the mean pressure minimum intensifies with $\beta = -1$. A noticeable thing by comparing Figs. 7(b) and 7(e) is that the distribution of instantaneous and mean pressure is similar. Thus, our counter-rotation model with $\beta = 1$ very effectively weakened the vortices and removes the pressure minimums and kind of makes the flow quasi steady, which can be further verified as shown in Fig. 8 by the instantaneous and mean velocity magnitude distribution. In addition, from Figs. 6 and 7, it can be drawn that the shedding period is basically unaffected by counter-rotation force model as the instantaneous distributions are in phase with each other.

Compared with the centripetal force models, clearly this second approach is more effective in alternating the flows since the centripetal force can be compensate by pressure gradient while the counter-rotation force directly modifies the velocity field. However, both models are helpful in understanding the flow mechanisms and can be used for different purposes. Just as for the first model, we can also

change the magnitude of β to see the control results. It has been stated that the time scale τ cannot be too small (correspondingly β too large) to cause numerical instability. If we select τ to be the time step of the numerical simulation 0.05, then $\beta = 20$, which make the simulation quickly diverge. Aside from that, the trend of variating β would not change the overall qualitative description above since it is basically an active closed loop control, i.e., wherever a vortex presents, forces will be applied to weaken or strengthen it.

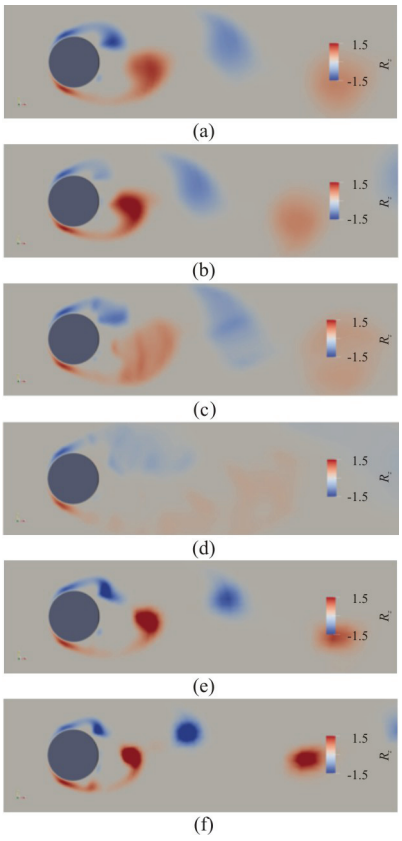

Fig. 6 (Color online) Counter-rotation model with $\beta = \pm 1$. The distribution of Liutex component R_z for the uncontrolled case in (a) and (b), and for the controlled case $\beta = 1$ in (c) and (d), and for the controlled case with $\beta = -1$ in (e) and (f). (a), (c) and (e) are at $t = t_0 + 0.096T$, while (b), (d) and (f) are at $t = t_0 + 1.92T$

Pair of counter-rotating vortices are often seen in nature and engineering. To study the interaction between pair vortices, we restrict the force field model to the clockwise rotating vortices in flow past the cylinder, while left anti-clockwise rotating vortices uncontrolled. As shown in Figs. 9(a) and 9(c) the upper clockwise vortices are weakened by counter-rotation force with $\beta = 1$. It can be inferred that weakening of the upper clockwise vortices also leads to weakening of downside anti-clockwise vortices. A scrutiny of Fig. 9(c) reveals that in average the vortices are not symmetric as the anti-clockwise vortices are stronger than clockwise ones. Similarly, with the upper vortices strengthened by force model, the downside vortices have also been intensified as shown in Figs. 9(b) and 9(d), and in average the clockwise vortices are stronger than the anti-clockwise vortices. These results mean that generally vortex pairs reinforce each other and strengthening one would intensify the other and weakening one would attenuate the other. The reason is that the fluid between vortex pair are flowing to the same direction, preventing these fluids from moving would attenuate both the vortices and vice versa.

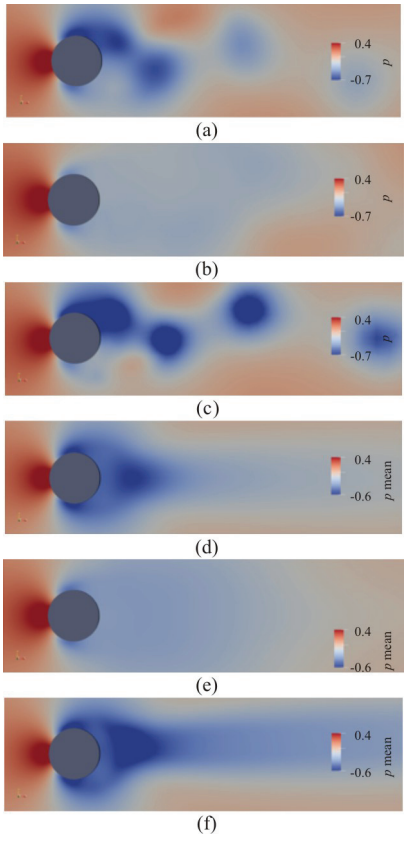

Fig. 7 (Color online) Counter-rotation model with $\beta = \pm 1$. The distribution of pressure and mean pressure for the uncontrolled case in (a) and (d), and for the controlled case $\beta = 1$ in (b) and (e), and for the controlled case with $\beta = -1$ in (c) and (f). (a), (b) and (c) are at $t = t_0 + 47.8T$, while (d), (e) and (f) are mean pressure distributions

In hydrodynamics, flow region of low pressure is dangerous and prone to cavitate if the pressure is low enough. In particular, vortex cavitation is the kind of

cavitation with low pressure caused by vortices. From the discussion above, maintaining an additional centripetal force could somehow attenuate the pressure minimum and thus might alleviate vortex cavitation.

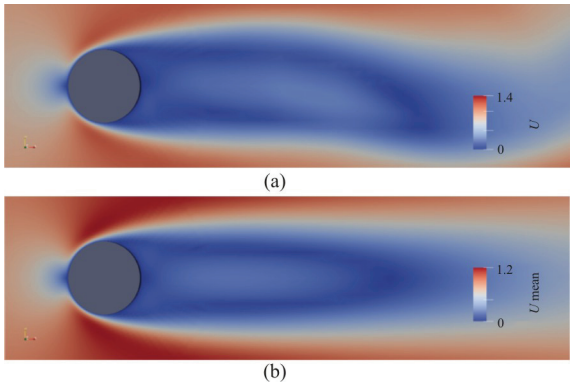

Fig. 8 (Color online) The instantaneous and mean velocity magnitude distribution: (a) $t = t_0 + 47.8T$ (b) time average

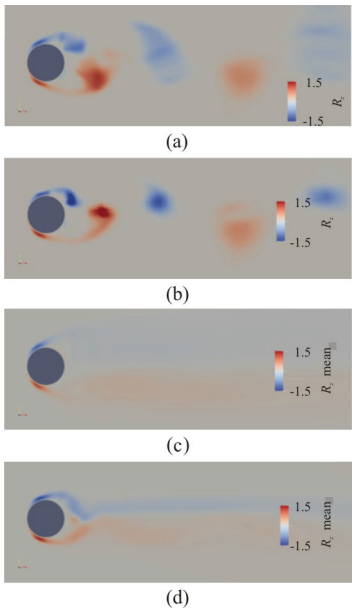

Fig. 9 (Color online) The instantaneous and mean Liutex distributions with only clockwise rotating vortices controled. $\beta = 1$ in (a) and (c) while $\beta = -1$ in (b) and (d). (a), (b) are at $t = t_0 + 0.096T$ while (c), (d) are mean distributions

4. Cavitating flow around two-dimensional Clark-Y hydrofoil

In this section, we use the numerical results of a cavitating Clark-Y hydrofoil to explore the relationship between vortex and cavitation in this particular flow, and explore the possibility of using the force models to control or alleviate cavitation. The Clark-Y hydrofoil, with chord length $c = 0.07$ m and angle of attack $a = 8°$ is used in the current research to investigate Liutex force field models. The computational domain is consistent with the experimental water tunnel of Huang and Wang[31] The incoming flow velocity is 10m/s and the cavitation number defined by the outlet pressure is 0.8. The simulation is implemented on OpenFOAM with the solver developed by Laboratory for Advanced Simulation of Turbulence (LAST) in Tsinghua University, including a novel cavitation model called nonlinear dynamic cavitation model (NDCM). For the reason of fundamental research, two-dimensional model is considered here, and the k-Ω- SST turbulence model is adopted.

It is shown in Fig. 10 that instantaneous contours of Liutex, volume of fraction of water α_w and the pressure, and five vortices are marked with squares and circles and labeled from 1 to 5. First the correspondence of these vortices and the pressure minimums is obvious, especially for vortices 1, 4 and 5, which are free from cavitation. Yu and Wang[27] have applied the centripetal force model and counter-rotation force model to a vortex similar to vortex 5 and obtained similar results as previous section. Clearly, in the wake flows vortices are relatively stable and can travel a long distance with encircled low-pressure minimum. On the other hand, just above the tail part of the hydrofoil lays vortices 2 and 3, where the flow is cavitating and the pressure is very low. Compared with the distribution of α_w in Fig. 10(b), the bubbles are actually in the center of vortices 2 and 3. However, the corresponding Liutex concentrations are located just around the cavitation bubbles, i.e., near the interface between water and air. Although cavitation is a very complicated phenomenon, and in the current numerical simulation, those $\alpha_w = 0$ areas contain countless smaller bubbles, which have been modeled rather than resolved, the trend that cavitation would induce vortex due to instability is clear as illustrated by vortices 2 and 3 with their centers void of Liutex. Based on current simulation, the mechanism in this particular flow could be summarized as with cavitation cloud formed, instability of the interface between water and air cloud leads to the formation of Liutex represented fluid rotation. As those Liutex circulated cavitation clouds convected downstream and shed off, wake vortices with low pressure centers are formed, which persist for a long distance.

Liutex, α_w and pressure distribution at a subsequent time step are shown in Fig. 11. We can see that although the cavitation bubbles have a very different shape from that in Fig. 10, the trend

described above that vortices form around the interface between water and cavitation clouds, also applies. In addition, the two vortices labeled 2 and 3 in Fig. 11 are actually vortices 2 and 3 in Fig. 10 convected downstream, which confirms the shedding off vortices are generally comes from the cavitation bubbles.

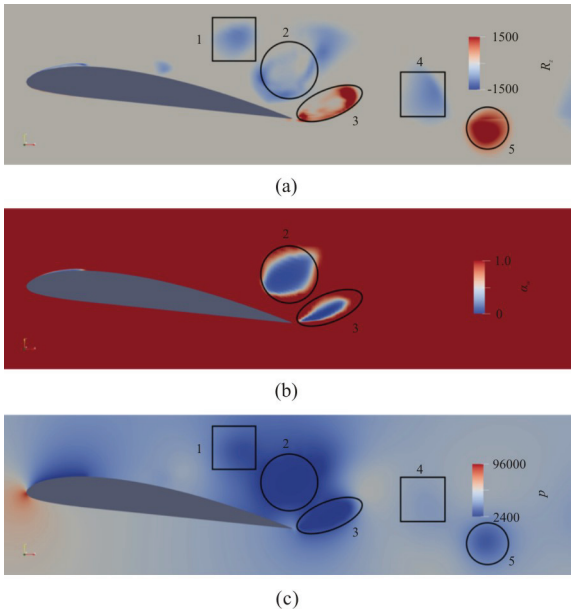

Fig. 10 (Color online) The instantaneous contours of (a) Liutex, (b) volume of fraction of water and (c) pressure

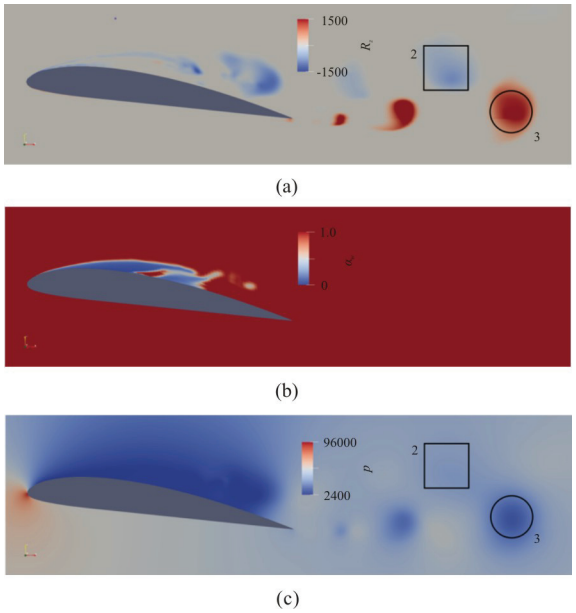

Fig. 11 (Color online) A subsequent instantaneous contours of (a) Liutex, (b) volume of fraction of water and (c) pressure

We now focus on the vortex circumscribed in Fig. 12, which has been shed off and encircles cavitation. During the time from which we denote $t = t_0$ to $t = t_0 + T/40$ with T as the period of the flow. It can be seen during the small time interval the vortex has been convected downstream, and the cavitation bubble inside the vortex still persist and even get a little larger. That is because the rotation speed has been increased which lead to a lower pressure inside the vortex and thus aggregate cavitation. With the centripetal force model, we use local maximum Liutex point as the vortex center, and set $\alpha = 2$ to make sure the increment of pressure inside the vortex is enough to alleviate cavitation. The force begins to take effect at $t = t_0$, and note that only the circumscribed vortex area is controlled. The distributions of Liutex, α_w and pressure at $t = t_0 + T/40$ are shown in Fig. 13. Obviously, the cavitation inside the vortex is basically eliminated, confirming the strategy is still usable even with cavitation. Quantitatively, the mean pressure over the vortex area increased from $p = 2\,000$ to $p = 15\,000$, which is larger than the saturated vapor pressure and thus eliminating cavitation. On the other hand, the magnitude of Liutex is basically unchanged by comparing Figs. 12(b), 13(a). It is thus understood that as the vortex sheds off from hydrofoil, the vortex rotates very fast and the very low pressure is sustained by requiring the centripetal force to balance. The results testify that cavitation induced low pressures have the tendency to create vortices whose centripetal force balances the strong pressure gradient.

The counter-rotation force model with $\beta = 80/T$ is also applied to control the same vortex, and the results are shown in Fig. 14. The cavitation is again effectively eliminated and pressure at the vortex center has been raised up to value larger than the saturated vapor pressure. A distinctive feature from Fig. 14 is that despite the rotation of the vortex center has been suppressed, the surrounding areas still possess significant magnitude of Liutex. The situation is that the counter-rotation force model is aimed at directly modifying the velocity field inside a vortex and thus eliminating Liutex. However, as the fluid rotation being controlled, the low pressure inside the vortex core again induces new rotation around the interface between the surrounding water and the vortex, which lead to the vortex shape in Fig. 14.

The two examples illustrate that Liutex-based vortex control might be utilized to suppress certain cavitation, at least in numerical simulations. Directly manipulating vortices by the centripetal force model or counter-rotation force model can be viewed as closed-loop control in numerical simulations, which certainly is very difficult to realize in practice. First, it is generally very hard to obtain information of the flow field away from the wall surface by sensors in

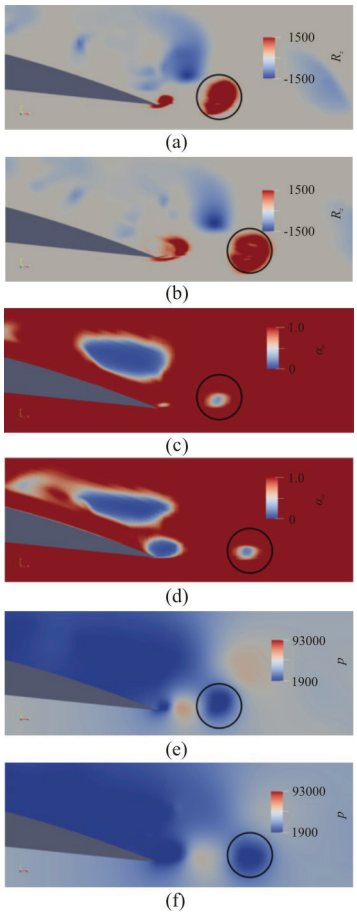

Fig. 12 (Color online) The distribution of Liutex component R_z, volume of fraction of water and pressure for the uncontrolled case. (a), (c) and (e) are at $t = t_0$, while (b), (d) and (f) at $t = t_0 + T / 40$

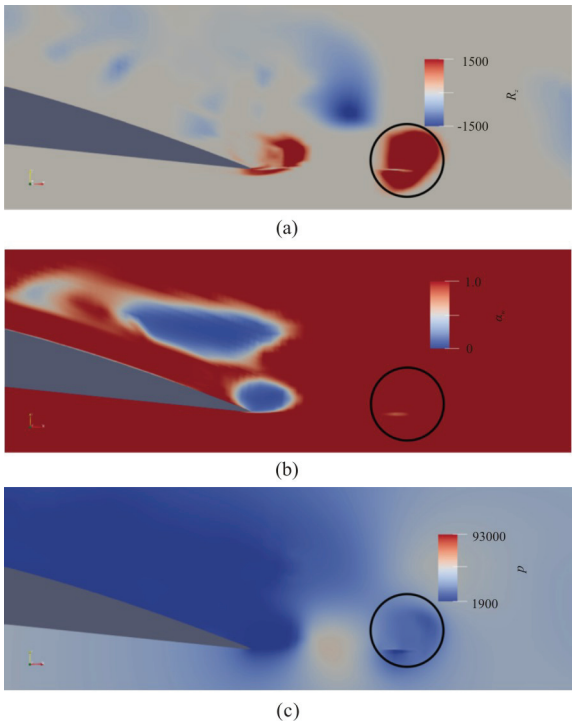

Fig. 13 (Color online) The distribution of Liutex component R_z, volume of fraction of water and pressure for centripetal force model controlled with $\alpha = 2$ at $t = t_0 + T / 40$

real time, which is necessary to calculate the force field. Second, to generate spatial forces calculated precisely pose great challenges in applications. Generally, we can only introduce sensors, devises on the wall surface. In addition, the Liutex-based vortex force field are to be applied in space since vortices cannot be placed on the wall due the no-slip condition. However, the current research is still of importance in the sense that first with Liutex-based force models employed in numerical simulations, we can study the vortex dynamics, which has been viewed as the skeleton of the flow, as in the examples provided above. For a flow under consideration, Liutex-based vortex force field models can strengthen or attenuate certain vortices, and even create vortices in designed places as we wish, of course, in numerical simulations. Comparing uncontrolled and the controlled cases might gain us deeper understanding of the flow mechanics. Second, although the application prospect of the methodologies in current research have been diminished, it might lead to applicable strategies. For example, as the centripetal model generally only mildly modifies the velocity field, and slightly modifies the shedding period, we may replace the closed-loop control to periodic active control, i.e., in the purpose of suppress the considered cavitating vortex above, we can apply a periodic centripetal force only in the spatial domain covered by the vortex during the time interval of $T / 40$. For the forces to be exerted spatially, DBD plasma actuator might be an option. In addition, strategies of suction and ejection control, and wall oscillation control might be guided by Liutex-based force field models. More specifically, cavitation is a complex phenomenon closely related to low pressure, which might be thought to be controlled by Liutex-based vortex force field models, since vortex is also concerned with low pressure centers. However, cavitation is unsteady, multi-phase, turbulence involving, whose mechanism has not been fully understood and hard to control. It would be of great importance if we can devise Liutex-based force field models to suppress cavitation in general rather than the particular cavitating bubbles eliminated in the examples, which still need further investigation.

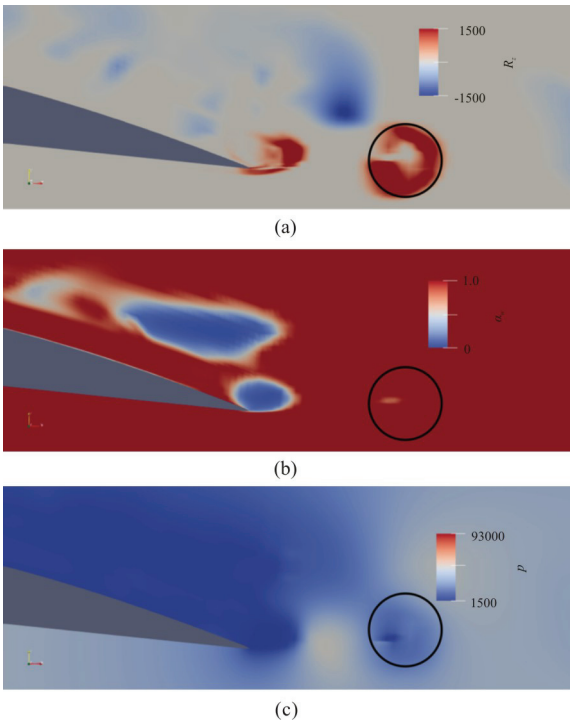

Fig. 14 (Color online) The distribution of Liutex component R_z, volume of fraction of water and pressure for counter-rotation force model controlled with $\tau = T/80$ (thus $\beta = 80/T$) at $t = t_0 + T/40$

5. Conclusions

Compared with previous scalar vortex identification methods, the third generation of vortex definition and identification system of Liutex has a much clearer physical meaning as its direction is the local rotation axis and its magnitude is the angular velocity of the rigid-body rotation part of the fluid motion. With the idea that vortex plays an important role in determining the flow mechanics, Liutex is the only possible vortex definition that could be directly used to extract a force field based on the six core elements. Two force field models, centripetal-force model and counter-rotation model, have been applied to a flow past a cylinder at Reynolds number of 200 and a cavitating flow around Clark-Y hydrofoil with cavitation number of 0.8. Conclusions have been drawn that the models are effective ways to modify the flow field with purposes of control vortices effectively. Especially, the relationship between vortices and pressure minimums and the mechanisms of vortex generation in cavitating flow are discussed. Generally, centripetal force control will relieve the pressure minimums inside vortices while mildly modifies the velocity field, and thus vortices. On the other hand, counter-rotation model is more effective in attenuating or eliminating vortices, and make the flow transforms towards some steady form. In addition, in the context of cavitating hydrofoil flow, the relationship among low pressures, vortices and cavitation bubbles are investigated. And for a vortex encircled cavitation bubble, the centripetal force model and counter-rotation force model have been proved to be effective in suppressing or eliminating the particular cavitation bubble.

Despite that both centripetal force field model and counter rotation force field model are applied in the form of a source term on the right-hand side of the Navier-Stokes equations, dynamics between them are rather different. A pressure minimum soothing centripetal force model would be generally applied perpendicular (or form acute angles significantly larger than zero) to the velocity direction, and attenuate the stretch between adjacent fluids in that the centripetal force needed for the fluids to rotate now provided by the force model rather than pressure gradient. On the other hand, the counter rotation force field model actually creates moment of force that stops the fluids from rotating. As the rotation of fluids, i.e., vortex, is killed or significantly attenuated, the severe pressure gradient to maintain centripetal forces is no longer needed, and thus low pressure that leads to cavitation could possibly be avoided. Selection between these two models relies on the application and the purpose of our control. Generally, the centripetal force field model is preferred if we are primarily focused on relax the pressure minimum, or control cavitation, but do not want to significantly change the flow field. On the other hand, if the main goal is to kill vortices, clearly the counter rotation force model is more effective.

Future directions include implementing Liutex-based vortex control methodologies in three-dimensional flow, which pose technical difficulties as in the direction of Liutex would be varying from point to point, thus leading to curved vortex core lines. In addition, in the present study, only incompressible flows are considered and thus pressure is only coupled with the velocity field. However, the effect compressibility and equation of state on the models need to be quantified. Due to the importance and complexity of the issue of cavitation in hydrodynamics, applicable cavitation suppression will serve as an ultimate goal, and certainly cavitation mechanisms and effective numerical force models should be further investigated.

Acknowledgment

Communications with Profs. Liandi Zhou, Chaoqun Liu, and Zheng Ma are highly appreciated.

References

[1] Luo X., Ji B., Tsujimoto Y. A review of cavitation in hydraulic machinery [J]. *Journal of Hydrodynamics*, 2016, 28(3): 335-358.

[2] Huang B., Qiu S. C., Li X. B. et al. A review of transient flow structure and unsteady mechanism of cavitating flow [J]. *Journal of Hydrodynamics*, 2019, 31(3): 429-444.

[3] Nakamura K., Kurosawa S. Design optimization of a high specific speed Francis turbine using multi-objective genetic algorithm [J]. *International Journal of Fluid Machinery and Systems*, 2009, 2(2): 102-109.

[4] Enomoto Y., Kurosawa S., Kawajiri H. Design optimization of a high specific speed Francis turbine runner [J]. *IOP Conference Series: Earth and Environmental Science*, 2012, 15(3): 032010.

[5] Che B., Chu N., Schmidt S. J. et al. Control effect of micro vortex generators on leading edge of attached cavitation [J]. *Physics of Fluids*, 2019, 31(4): 044102.

[6] Che B., Chu N., Cao L. et al. Control effect of micro vortex generators on attached cavitation instability [J]. *Physics of Fluids*, 2019, 31(6): 064102.

[7] Küchemann D. Report on the I.U.T.A.M. symposium on concentrated vortex motions in fluids [J]. *Journal of Fluid Mechanics*, 1965, 21(1): 1-20.

[8] Liu C., Yan Y., Lu P. Physics of turbulence generation and sustenance in a boundary layer [J]. *Computers and Fluids*, 2014, 102: 353-384.

[9] Liu C., Gao Y. S., Dong X. R. et al. Third generation of vortex identification methods: Omega and Liutex/Rortex based systems [J]. *Journal of Hydrodynamics*, 2019, 31(2): 205-223.

[10] Robinson S. K. Coherent motion in the turbulent boundary layer [J]. *Annual Review of Fluid Mechanics*, 1991, 23: 601-639.

[11] Wang Y., Yang Y., Yang G. et al. DNS study on vortex and vorticity in late boundary layer transition [J]. *Communications in Computational Physics*, 2017, 22(2): 441-459.

[12] Hunt J., Wray A., Moin P. Eddies, streams, and convergence zones in turbulent flows [R]. Proceedings of the Summer Program. Center for Turbulence Research Report CTR-S88, 1988, 193-208.

[13] Jeong J., Hussain F. On the identification of a vortex [J]. *Journal of Fluid Mechanics*, 1995, 285: 69-94.

[14] Chong M. S., Perry A. E., Cantwell B. J. A general classification of three-dimensional flow fields [J]. *Physics of Fluids A*, 1990, 2(5): 765-777.

[15] Zhou J., Adrian R., Balachandar S. et al. Mechanisms for generating coherent packets of hairpin vortices in channel flow [J]. *Journal of Fluid Mechanics*, 1999, 387: 252-296.

[16] Liu C., Gao Y., Tian S. et al. Rortex-A new vortex vector definition and vorticity tensor and vector decompositions [J]. *Physics of Fluids*, 2018, 30(3): 034103.

[17] Liu J., Gao Y., Liu C. An objective version of the Rortex vector for vortex identification [J]. *Physics of Fluids*, 2019, 31(6): 065112.

[18] Dong X., Gao Y., Liu C. New normalized Rortex/vortex identification method [J]. *Physics of Fluids*, 2019, 31(1): 011701.

[19] Liu J., Liu C. Modified normalized Rortex/vortex identification method [J]. *Physics of Fluids*, 2019, 31(6): 061704.

[20] Gao Y., Liu J., Yu Y. et al. A Liutex based definition of vortex rotation axis line [J]. *Journal of Hydrodynamics*, 2019, 31(3): 445-454.

[21] Xu H., Cai X. S., Liu C. Liutex (vortex) core definition and automatic identification for turbulence vortex structures [J]. *Journal of Hydrodynamics*, 2019, 31(5): 857-863.

[22] Wang Y. Q., Gao Y. S., Xu H. et al. Liutex theoretical system and six core elements of vortex identification [J]. *Journal of Hydrodynamics*, 2020, 32(2): 197-211.

[23] Liu C., Gao Y. Liutex-based and other mathematical, computational and experimental methods for turbulence structure [M]. Sharjah, United Arab Emirates: Benthom Science Publishers, 2020.

[24] Liu C., Xu H., Cai X. et al. Liutex and its applications in turbulence research [M]. Cambridge, Massachusetts, USA: Academic Press, 2020.

[25] Vainchtein D., Meziç I. Vortex-based control algorithms (Koumoutsakos P., Meziç I. Controlof fluid flow. Lecture notes in control and information sciences) [M]. Berlin, Germany: Springer, 2006.

[26] Protas B. Vortex dynamics models in flow control problems [J]. *Nonlinearity*, 2008, 21(9): 203-250.

[27] Yu H. D., Wang Y. Q. Liutex-based vortex dynamics: A preliminary study [J]. *Journal of Hydrodynamics*, 2020, 32(6): 1217-1220.

[28] Gao Y., Liu C. Rortex and comparison with eigenvalue-based vortex identification criteria [J]. *Physics of Fluids*, 2018, 30(8): 085107.

[29] Wang Y. Q., Gao Y. S., Liu J. M. et al. Explicit formula for the Liutex vector and physical meaning of vorticity based on the Liutex-Shear decomposition [J]. *Journal of Hydrodynamics*, 2019, 31(3): 464-474.

[30] Braza M., Chassaing P., Minh H. Numerical study and physical analysis of the pressure and velocity fields in the near wake of a circular cylinder [J]. *Journal of Fluid Mechanics*, 1986, 165: 79-130.

[31] Huang B., Wang G. Y. Partially averaged Navier-Stokes method for time-dependent turbulent cavitating flows [J]. *Journal of Hydrodynamics*, 2011, 23(1): 26-33.